Advanced Steel Construction – Vol. 19 No. 1 (2023) 52–69
DOI:10.18057/IJASC.2023.19.1.8
(**Special Issue:** *10th International Conference on Advances in Steel Structures, ICASS'2020, Chengdu, China*)

BEHAVIOR OF WEB PERFORATED COLD-FORMED STEEL BEAMS UNDER COMBINED BENDING AND SHEAR ACTION

Li-Ping Wang [1, 2, *], Jian Li [1], Xing-Xing Cao [1], Dong-Hui Wen [3] and Hai-Bo Wang [4]

[1] *School of Civil Engineering, Central South University, Changsha 410075, PR China*
[2] *Engineering Technology Research Center for Prefabricated Construction Industrialization of Hunan Province, Changsha, 410075, PR China*
[3] *Department of Architecture and Environmental Engineering, Taiyuan University, Taiyuan 030032, PR China*
[4] *Hunan Tieyuan Civil Engineering Testing Co., Ltd, Changsha 410075, PR China*
** (Corresponding author: E-mail: wlp2016@csu.edu.cn)*

ABSTRACT

To cater engineering application needs, cold-formed steel (CFS) members often have some web openings which could influence bearing capacity of the steel beam under combined bending and shear action. This paper presents tests on 20 groups of thin-walled web-perforated lipped C-shaped CFS beams, which were conducted under single point loading mode at mid-span. Besides, detailed finite element parameter analysis on the high shear-span ratio (a/h= 1.5 ~ 4.0) specimens was conducted by ABAQUS after the model was verified, which was mainly focused on the influences of different hole depth-to-web height ratios (d_h/h) and web height-to-thickness ratios (h/t) on the bearing capacity and failure modes of the beams. Based on the results of test and FEA, the mechanical behavior and failure rules of thin-walled web perforated lipped C-shaped CFS beams under combined bending and shear action were deeply studied.

ARTICLE HISTORY

Received: 20 July 2022
Revised: 22 August 2022
Accepted: 10 January 2023

KEYWORDS

Cold-formed steel;
Combined action of bending and shear;
Web openings

1. Introduction

The thin-walled web-perforated CFS members are commonly used in practical engineering applications to provide convenience for the installation of pipeline facilities and to achieve efficient use of story height. However, the web opening will result in an unfavorable effect in the mechanical performance of the members. A series of research had been done on the behavior of web-perforated CFS members. From 1994 to 1997, Langan et al. [1-3] carried out experimental and theoretical research on web perforated flexural CFS members, a series of shear capacity design formulas for CFS members with web perforations (including circular holes and non-circular holes) were proposed, which have been adopted in AISI S100 [4] and AS/NZS 4600 [5]. Through experimental and theoretical research on thin-walled CFS flexural and compression members, Schafer et al. [6-9] put forward a new method taking interactive buckling of plates into consideration to calculate the bearing capacity of thin-walled CFS members, namely the direct-strength-method (DSM). In 2004, the direct-strength-method (DSM) was adopted by the AISI S100 [4]. In 2008, Moen et al. [10-13] proposed the modified DSM formula for CFS beams with web openings after experimental and theoretical research on web-perforated CFS flexural members. In 2012, on the basis of test results of plain lipped CFS members with C-shaped and Supa-Cee section, Pham and Hancock [14] proposed specific DSM for C-shaped steel beams in shear and in combined bending and shear action, in which the influence of tension field action was considered. In 2014, Keerthan et al. [15,16] conducted test and FEA on the hollow flange channel beams under combined bending and shear action, and proposed the lower bound equation applicable to the section form. In 2015, by means of test and FEA, Faridmehr [17] et al. studied behavior of C-channel stiffened CFS beams subjected to the bending and the primarily shear conditions, verified the effectiveness of the stiffening design, and pointed out the conservatism of M-V interaction design method in AISI. For double limb built-up section CFS bending members, Young and Wang [18,19] carried out series of tests and FEA studies during 2015 to 2017, and extended the rules of DSM for these members with the effect of openings and screws considered. During 2018 to 2019, Pham [20,21] et al. used a new experiment setup to minimize effect of applied bending moment in shear span, so as to study shear capacity of CFS beams in higher aspect ratios, and the results from test were recalibrated with the theoretical calculation results of the DSM in AISI and AS/NZS. Degtyareva et al. [22] conducted FEA on thin-walled CFS bending members with staggered slotted web perforations under combined bending moment and shear force action in 2019, and put forward specific equations for the bearing capacity of this kind of members. For C-shaped web perforated beams, Lawson et al. [23] proposed a derived formula for calculating the additional deflection, and compared the calculating results with those of tests and FEA. In 2020, based on the test results of rectangular and slotted web perforations of high-strength CFS beams, Pham et al. [24] proposed a modified formula for the DSM design for this kind of members. In 2022, Wang et al. [25] conducted tests on 26 groups of thin-walled web-perforated CFS members with low shear-span ratio (1.0 and 1.5) and presented detailed finite element analysis, and the study was focused on the influence of holes on the shear performance of such members.

In this paper, to study the behavior of thin-walled web perforated lipped C-shaped CFS beams under combined bending moment and shear force action, tests on 20 groups of specimens were carried out, in which the single-point loading mode at mid-span section was adopted. And FEA was conducted by means of ABAQUS. The results of FEA and test were compared together, from which the accuracy of FEA model was validated. After that, by changing the hole depth-to-web height ratio and the web height-to-thickness ratio of the steel beams in relatively higher shear-span ratio (1.5 ~ 4.0), the parameter analysis was presented, and the effect of each parameter on the bending and shear performance of thin-walled web perforated lipped C-shaped CFS beams was deeply studied.

2. Experimental investigation of beams in bending and shear

2.1. Specimen design

The material of the 20 groups of specimens was all high strength zinc-coated cold-formed steel (G550), and section thickness was all 1.9 mm. Fig.1 (a) shows the dimension definition of the specimen. The specific meanings of each letter are as follow: the nominal web height is h, the nominal flange width is b_f, and the nominal lip width is b_l. Three different shear-span ratios of 2.0, 2.5 and 3.0 were designed in the test. The position of circular holes were all set at the half height of the specimen web within the shear zone, as shown in Fig.1 (b). The range of the value of d_h/h was 0 to 0.8. The label defining rules of specimen is presented in Fig. 2, in which repeated specimens are marked with R at the end of label. The dimensions of the specimen are presented in Table 1.

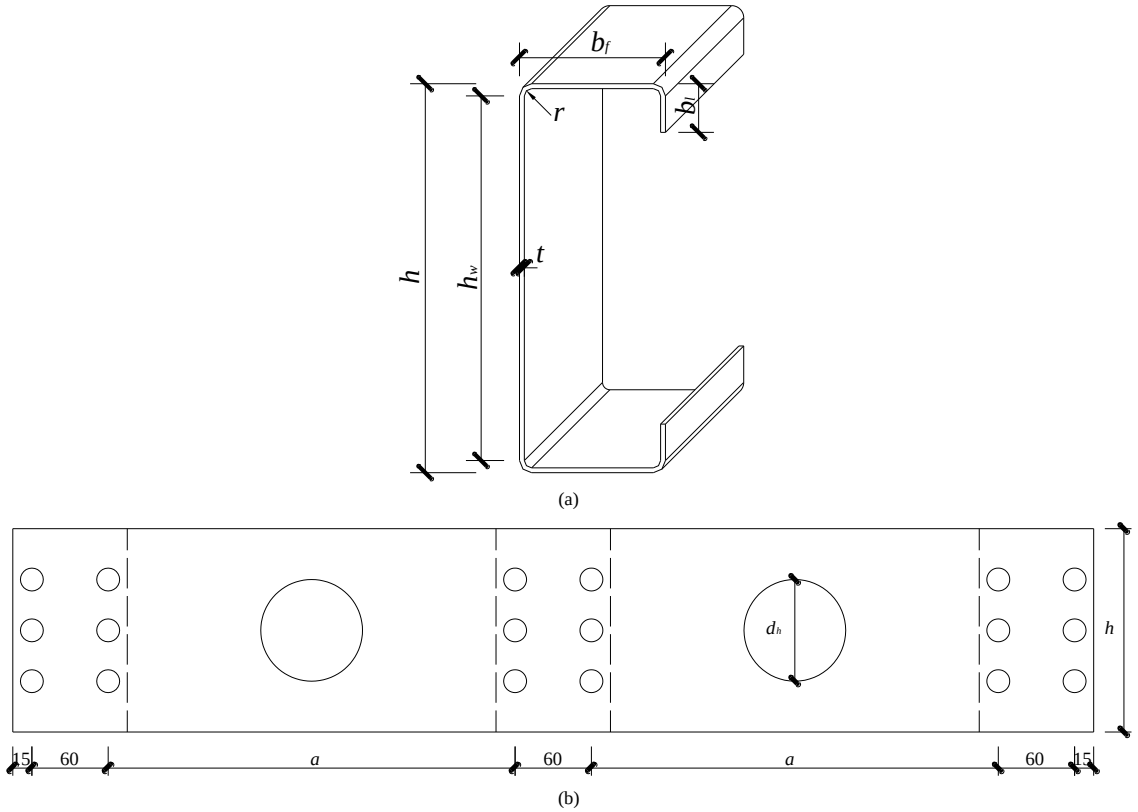

Fig. 1 Geometrical parameter definition (a) Section (b) Specimen

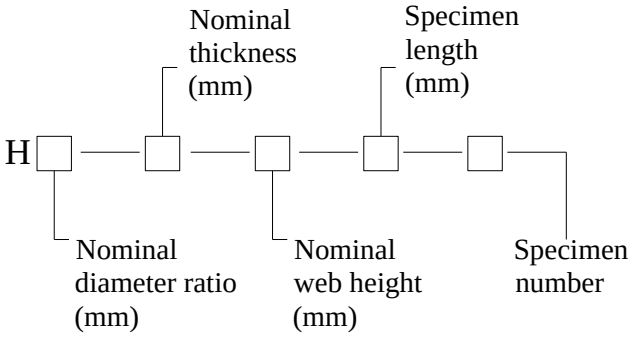

Fig. 2 Specimen labelling rules

Table 1
Geometric dimensions of specimen

Specimen	Web h_w/mm	Flange b_f/mm	Lip b_l/mm	Thickness t/mm	Diameter d_h/mm	The hole depth-to-web height ratio dh/h	The shear-span ratio a/h	The web height-to-thickness ratio h/t
H0-1.9-160-850-a	150.09	60.46	20.21	1.93	\	\		82.91
H0-1.9-160-850-b	150.17	60.39	20.38	1.92	\	\		83.34
H0-1.9-160-850R-a	150.30	60.73	20.45	1.93	\	\		82.95
H0-1.9-160-850R-b	151.36	60.59	20.46	1.91	\	\		83.66
H0.35-1.9-160-850-a	150.21	60.55	20.50	1.91	55.95	0.35	2.0	83.75
H0.35-1.9-160-850-b	149.97	60.57	20.42	1.90	55.83	0.35		84.13
H0.5-1.9-160-850-a	150.03	60.57	20.46	1.92	80.02	0.50		83.21
H0.5-1.9-160-850-b	150.40	60.66	20.45	1.91	79.97	0.50		83.58
H0.8-1.9-160-850-a	150.79	60.42	20.39	1.91	127.92	0.80		83.66
H0.8-1.9-160-850-b	149.85	60.56	20.26	1.91	127.92	0.80		83.52
H0-1.9-160-1010-a	150.47	60.69	20.37	1.92	\	\		83.48
H0-1.9-160-1010-b	150.76	60.49	20.46	1.90	\	\		84.28
H0.35-1.9-160-1010-a	150.74	60.73	20.33	1.95	55.88	0.35	2.5	82.23
H0.35-1.9-160-1010-b	150.60	60.45	20.61	1.94	55.89	0.35		82.47
H0.5-1.9-160-1010-a	150.36	60.44	20.45	1.91	80.03	0.50		83.66
H0.5-1.9-160-1010-b	150.04	60.35	20.40	1.93	80.01	0.50		83.08

H0.8-1.9-160-1010-a	150.72	60.80	20.96	1.88	128.03	0.81		84.35
H0.8-1.9-160-1010-b	150.63	61.44	20.92	1.91	128.02	0.81		83.18
H0-1.9-160-1170-a	150.68	60.55	20.44	1.96	\	\		81.96
H0-1.9-160-1170-b	152.56	60.59	19.94	1.93	\	\		83.29
H0-1.9-160-1170R-a	150.28	60.66	20.35	1.95	\	\		82.28
H0-1.9-160-1170R-b	150.40	60.72	20.30	1.96	\	\		81.76
H0.5-1.9-160-1170-a	151.23	61.61	19.80	1.94	79.98	0.49	3.0	83.57
H0.5-1.9-160-1170-b	151.24	60.77	19.82	1.92	79.97	0.50		83.48
H0.65-1.9-160-1170-a	150.53	60.66	21.22	1.90	104.04	0.65		83.93
H0.65-1.9-160-1170-b	151.04	60.56	20.47	1.95	104.05	0.65		82.02
H0.8-1.9-160-1170-a	150.86	60.65	19.91	1.99	127.92	0.80		80.73
H0.8-1.9-160-1170-b	151.18	60.73	19.95	1.97	127.91	0.80		81.61
H0-1.9-200-1010-a	193.69	74.67	24.43	1.93	\	\		103.48
H0-1.9-200-1010-b	193.94	74.66	24.24	1.94	\	\		103.06
H0.2-1.9-200-1010-a	193.41	74.69	25.00	1.92	39.98	0.20		104.22
H0.2-1.9-200-1010-b	193.59	74.67	24.77	1.90	39.89	0.20		105.32
H0.35-1.9-200-1010-a	193.85	74.65	24.95	1.92	69.92	0.35		104.41
H0.35-1.9-200-1010-b	1.93.40	74.74	24.91	1.91	69.90	0.35		105.03
H0.5-1.9-200-1010-a	193.91	74.67	24.49	1.93	99.87	0.50	2.0	103.96
H0.5-1.9-200-1010-b	194.32	74.64	24.89	1.89	99.95	0.50		106.37
H0.65-1.9-200-1010-a	193.15	74.63	24.88	1.90	129.92	0.65		105.20
H0.65-1.9-200-1010-b	193.35	74.90	25.32	1.92	129.91	0.65		104.21
H0.8-1.9-200-1010-a	194.25	74.76	24.62	1.90	159.95	0.80		104.98
H0.8-1.9-200-1010-b	193.68	74.71	24.92	1.91	159.87	0.80		104.61

2.2. Test program

In the test, the method of single-point loading at the load connector at the mid-span of a pair of specimens was adopted, which can avoid possible lateral deformation during loading. Fig. 3 shows the loading device of test. To adapt to loading needs of different-length specimens, two supports will move according to the specimen length, while reaction frame and reaction beam stayed at the original position.

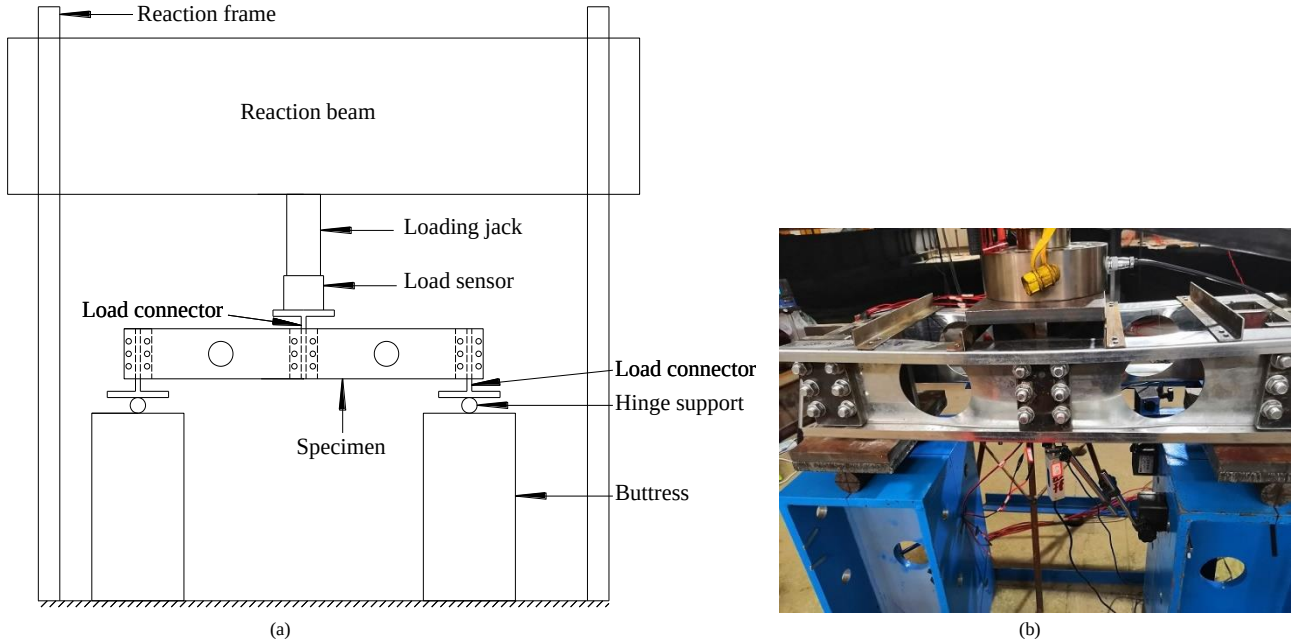

Fig. 3 Test loading device (a) sketch (b) Test photo

As shown in Fig. 4, for the alignment check before loading stage and the stress monitoring during the test, 5 strain gauges were set at compression flange and lip at mid-span of specimen and junction part of flange and web in tension. As can be seen in Fig. 5, to monitor the mid-span deflection, the out-of-plane bending deformation, the shear deformation and the distortional deformation, different transducers of displacement were set respectively.

For the purpose of evenly distributing the load to the two specimens, geometric alignment and physical alignment were all carried out before the tests. After the alignment was checked, the preloading was conducted, from which effect of inaccuracy specimen installation on the results can be eliminated. After 3 times of preloading, the formal loading was carried out. During the initial formal loading, the mode was controlled by force, then it was transformed into the displacement-control mode until the end of test. With safety ensured, the test was carried on after the maximum value of load to get complete load-displacement results.

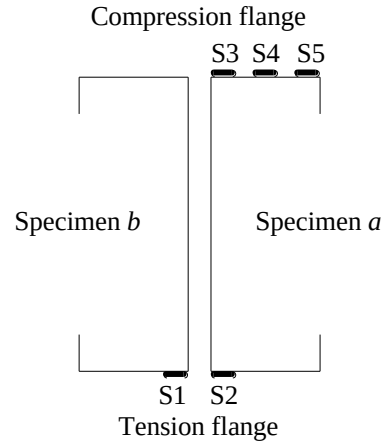

Fig. 4 Strain gauge arrangements

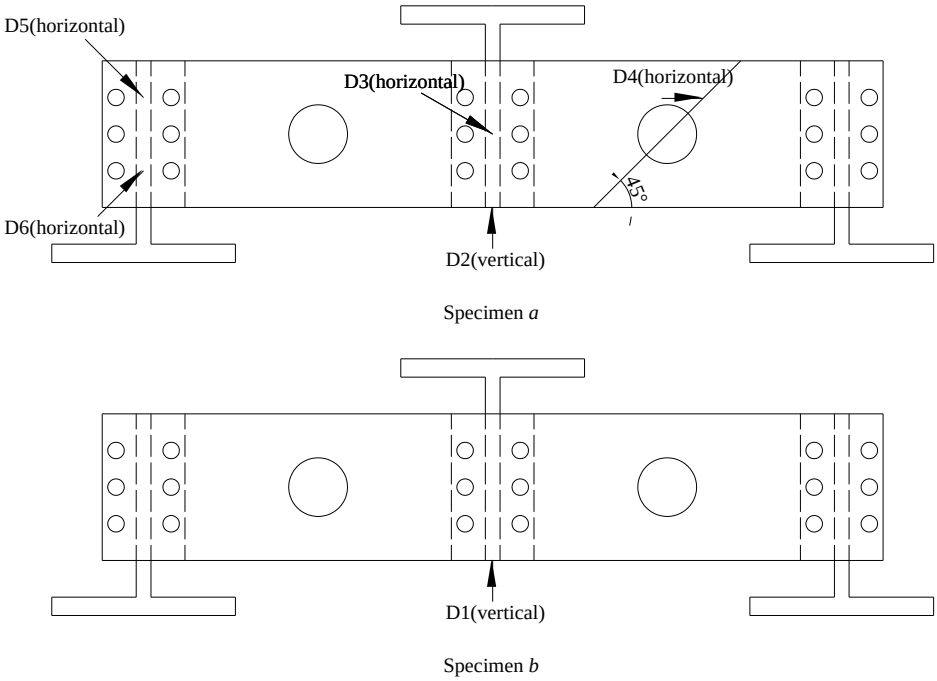

Fig. 5 Displacement meter arrangements

Table 2
Results from test and FEA

Specimen	Test results				The shear-span ratio	Reduction coefficient of F_u	Finite element results	V_{EXP}/V_{FEA}
	Ultimate bearing capacity	Mid-span moment	Shear force of central section of circular hole	Failure mode				
	F_u/kN	M_u/kN·m	V_{EXP}/kN		a/h	Δ	V_{FEA}/kN	
H0-1.9-160-850	87.41	15.30	43.71	D+L	2.0	1.00	39.45	1.11
H0-1.9-160-850R	87.54	15.32	43.77	D+L		1.00	39.45	1.11
H0.35-1.9-160-850	82.99	14.53	41.50	S+D+L		0.95	39.98	1.04
H0.5-1.9-160-850	65.54	11.47	32.77	S+D		0.75	32.47	1.01
H0.8-1.9-160-850	28.03	4.90	14.01	S		0.32	14.09	0.99
H0-1.9-160-1010	72.12	15.51	36.06	D+L	2.5	1.00	33.87	1.06
H0.35-1.9-160-1010	71.48	15.37	35.74	S+D+L		0.99	34.37	1.04
H0.5-1.9-160-1010	65.26	14.03	32.63	S+D		0.90	31.58	1.03
H0.8-1.9-160-1010	25.51	5.48	12.75	S		0.35	14.00	0.91
H0-1.9-160-1170	64.00	16.32	32.00	D+L	3.0	1.00	29.16	1.10
H0-1.9-160-1170R	63.64	16.23	31.82	D+L		1.00	29.16	1.09
H0.5-1.9-160-1170	61.87	15.78	30.94	S+D+L		0.97	29.99	1.03
H0.65-1.9-160-1170	44.93	11.46	22.47	S		0.70	22.32	1.01

H0.8-1.9-160-1170	27.76	7.08	13.88	S	0.43	13.93	1.00
H0-1.9-200-1010	94.99	20.43	47.50	D+L	1.00	44.79	1.06
H0.2-1.9-200-1010	91.60	19.69	45.80	D+L	0.96	45.37	1.01
H0.35-1.9-200-1010	93.37	20.07	46.68	S+D+L	0.98	44.26	1.05
H0.5-1.9-200-1010	73.52	15.81	36.76	S	0.77	35.65	1.03
H0.65-1.9-200-1010	49.73	10.69	24.87	S	0.52	25.36	0.98
H0.8-1.9-200-1010	29.73	6.39	14.87	S	0.31	15.19	0.98
						Average	1.03
						COV	0.048

2.0

2.3. Test results and discussion

2.3.1. Ultimate bearing capacity

Ultimate bearing capacity of specimen is listed in Table 2. Since stress condition and failure mode are the same for specimen in the same group, only results of specimen a were listed in the table.

By comparing with solid web specimen with the same value of a/h, the reduction coefficient in Fig. 6 of bearing capacity of web perforated specimen is obtained and shown in the column of Δ in Table 2. As can be seen from Fig. 6, variation of bearing capacity is inversely proportional to variation of the size of the opening. As the value of d_h/h increases from 0 to 0.8, for specimen with the value of a/h of 2.0, the bearing capacity of specimen decreases by 68% (h/t = 84.2) and 75% (h/t = 105.3), respectively. For specimen with the value of a/h of 2.5, the ultimate bearing capacity decreases by 65% (h/t = 84.2). And for specimen with the value of a/h of 3.0, the ultimate bearing capacity decreases by 57% (h/t = 84.2).

The relation of bearing capacity with the value of h/t is shown in Fig. 7. It can be seen from the figure, when the value of a/h and d_h/h of the specimen are constant, the higher the value of h/t is (the larger the effective shearing web area is), the greater the bearing capacity is. Under same conditions, the degree of effect of the value of h/t on the bearing capacity decreases as the hole diameter increases.

2.3.2. Load-deflection curves

The symmetrically set up pair of specimens and had basically same stress conditions and displacements, to facilitate the presentation and analysis, only load-deflection curves of specimen *a* are presented, as shown in Fig. 8. When the value of d_h/h is relatively smaller ($d_h/h \leq 0.5$), the curve has a rapid decrease after the maximum point. When the value of d_h/h is relatively larger ($d_h/h \geq 0.65$), the curve decreases more gently after the maximum point.

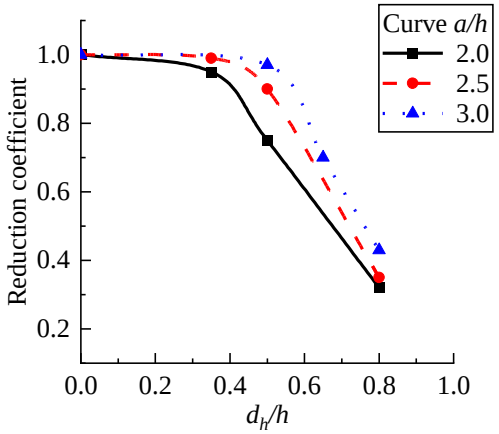

Fig. 6 Reduction coefficient of bearing capacity with the value of d_h/h

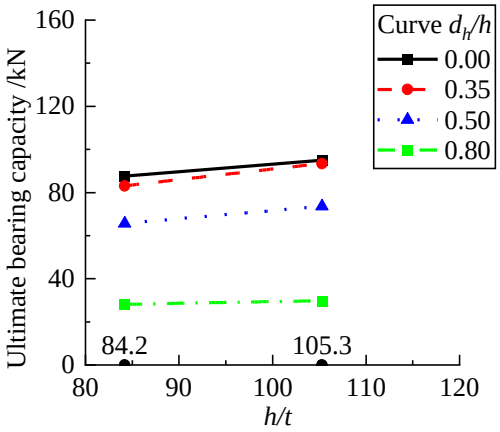

Fig. 7 Bearing capacity with the value h/t (a/h=2.0)

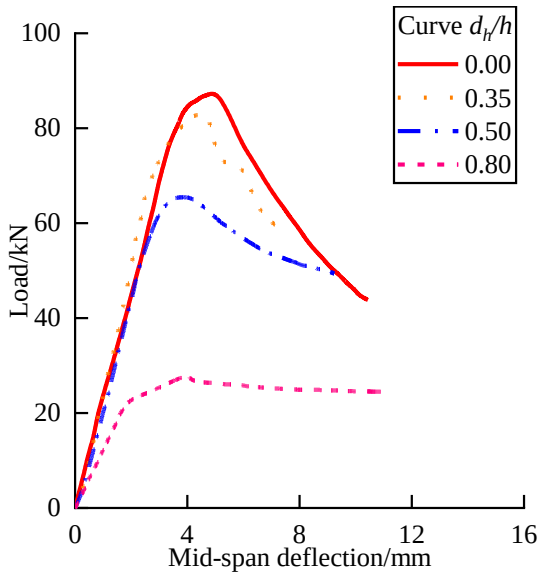

(a) Section H160-850 series

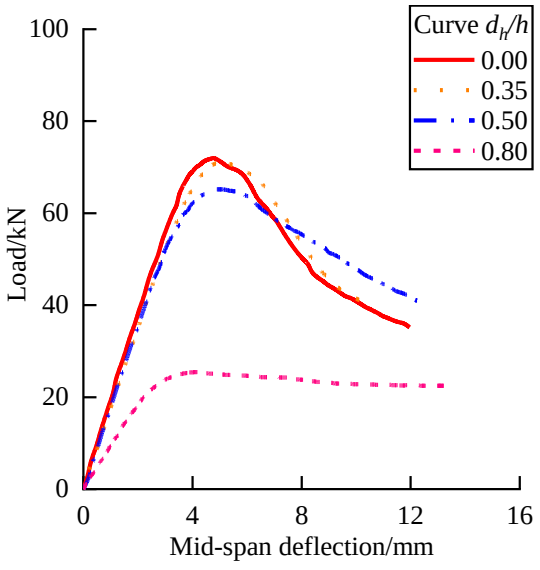

(b) Section H160-1010 series

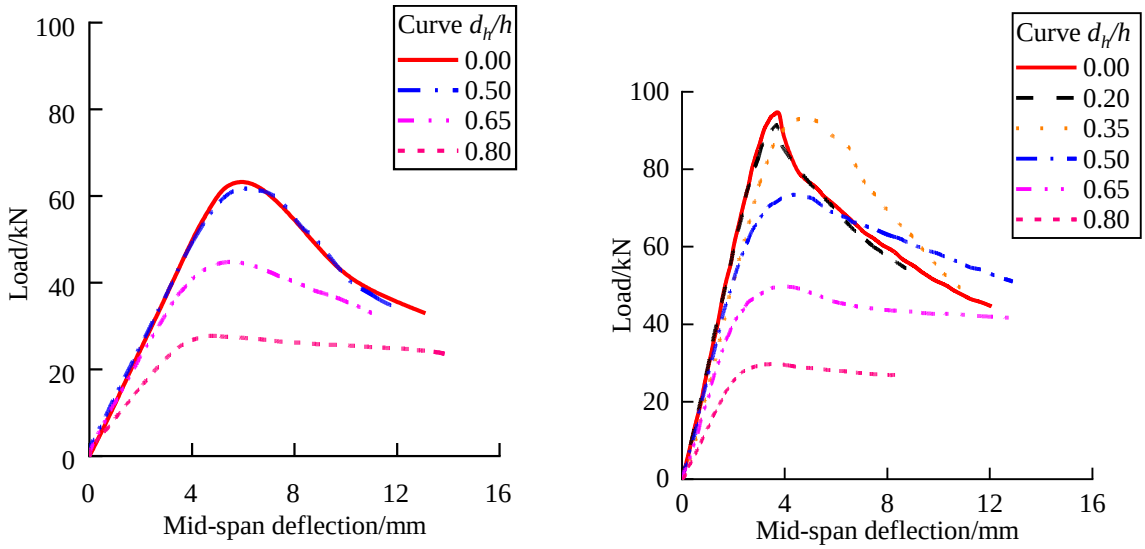

(c) Section H160-1170 series (d) Section H200-1010 series

Fig. 8 Load-deflection curves of specimen at mid-span

2.3.3. *Failure mode*

Since the specimens were under combined of bending moment and shear force action, there would be the bending failure mode dominated by local buckling deformation and distortional buckling deformation or shear failure mode dominated by the shear buckling deformation appear in the specimens. The failure mode is listed in Table 3 and shown in Fig 9.

Table 3
Failure mode of specimen

The value of a/h	Range of the value of d_h/h	Failure mode
a/h = 2.0	$d_h/h < 0.35$	The coupled failure of local buckling deformation and flange distortional buckling deformation.
a/h = 2.5		
a/h = 3.0	$d_h/h < 0.5$	
a/h = 2.0	$d_h/h = 0.35$	The shear buckling failure in web, accompanied by the coupled failure of local buckling deformation and flange distortional buckling deformation.
a/h = 2.5	$0.35 \le d_h/h \le 0.5$	
a/h = 3.0	$d_h/h = 0.5$	
a/h = 2.0	$d_h/h \ge 0.5$	The dominating web shear buckling failure.
a/h = 2.5	$d_h/h > 0.5$	
a/h = 3.0		

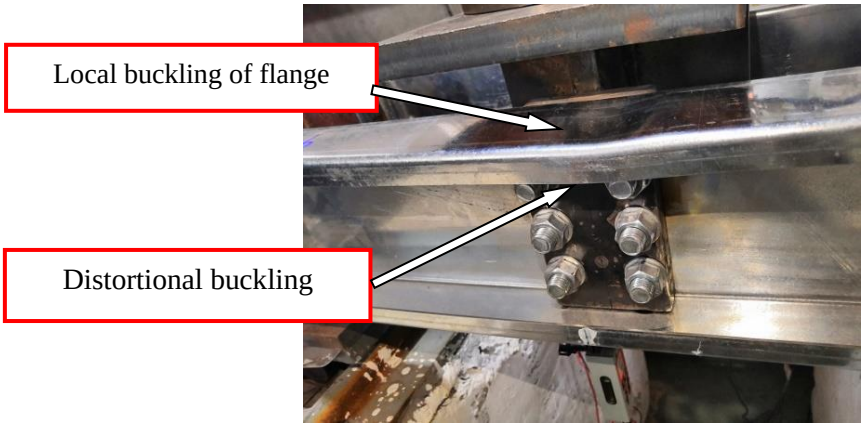

(a) Failure mode of specimen “H0-1.9-160-850”

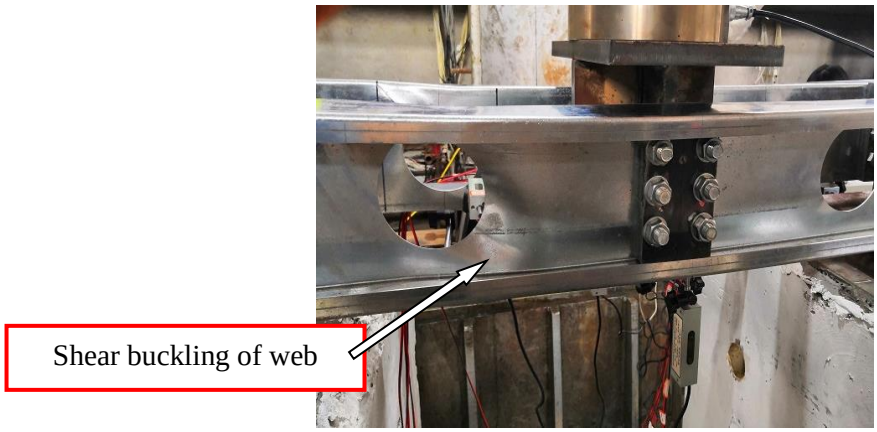

(b) Failure mode of specimen " H0.65-1.9-160-1170"

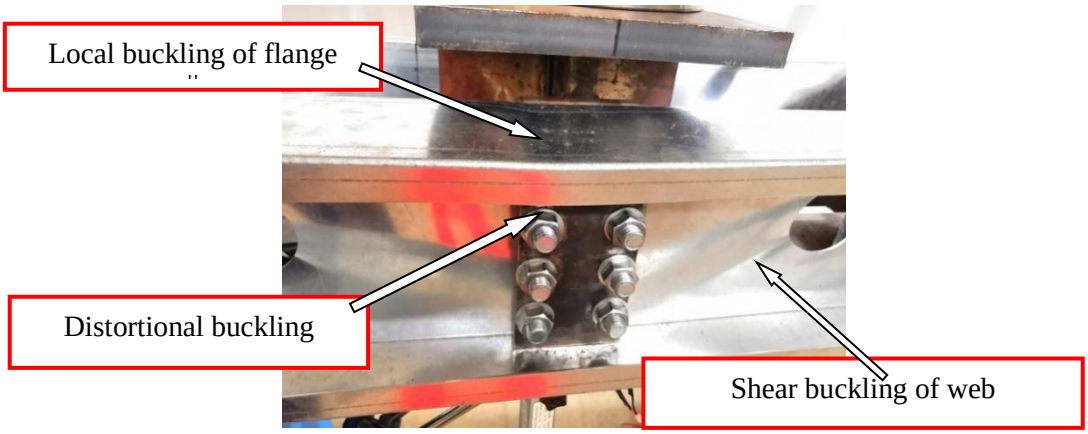

(c) Failure mode of specimen "H0.35-1.9-200-1010"

Fig. 9 Typical failure modes of specimens

3. Finite element analysis

3.1. Finite element model

The FEA model of specimen was established by means of ABAQUS. According to the test loading method, the model for FEA could be simplified by establishing only the model of specimen *a*.

3.1.1. Element and mesh

Due to that plate of lipped C-shaped CFS member is thin-walled shell, which is prone to produce buckling deformation, S4R shell element was adopted. The FEA models were divided into the meshing scale of 5×5 mm. For the model of web perforated specimens, area partition was conducted near the web hole in order to apply the quadrilateral mapped mesh, so as to ensure the convergence of calculation. Finally, the global mesh was divided.

3.1.2. Boundary conditions and loading mode

In response to the actual conditions in test, the setting of boundary condition in FEA model was as follows: at both ends of beam, where the supports were, coupling point was taken below the beam section to couple with the contact part between web and connector. At mid-span section, another point at the upper web (loading position) of the specimen was also taken to couple with the contact part. The displacement loading mode was adopted in FEA, and mid-span coupling point was adopted as load applying point, and Y direction displacement was applied at the point.

3.1.3. Material properties and initial imperfections

The specimen could obtain initial imperfections due to the effect of manufacture or other factors, which can affect the mechanical performance of specimen. The material properties of the specimen obtained through the tensile test are shown in Table 4, and it was applied in the finite element model according to setting rules of ABAQUS. For the specimens with value of *h*/*t* of 52.6, 84.2 and 105.3, the measured initial imperfection was 0.588 mm, 0.892 mm and 0.887 mm, respectively.

Table 4
Material properties

Nominal strength of yield point	Other parameters			
$\sigma_{0.2}$/ MPa	E/ GPa	$\sigma_{0.2}$/ MPa	σ_u/ MPa	ε_f/ %
550.00	200.90	574.30	607.00	12.28

3.1.4. Analysis method

The overall finite element analysis process used a two-step approach, namely the eigenvalue buckling analysis step and the nonlinear analysis step. During first one step, the required buckling modes were extracted. And on basis of that, in the second step, the measured initial imperfections were added and applied in analysis. To achieve smooth convergence of nonlinear analysis process, it was further divided into halves. Number one was to ensure the smooth operation of boundary conditions and contact relations by appliance of small value of displacement, and number two was to apply all the displacements to the specimen.

3.2. Model validation against test results

For the FEA model validation, it was conducted by comparing results of FEA and test together, respectively from the following aspects: the failure mode, the ultimate bearing capacity and the load-deflection curve.

3.2.1. Failure characteristics

The failure mode of specimen from FEA and test are compared in Fig. 10. As seen from the figure that the failure mode of the FEA is generally consistent with that of test.

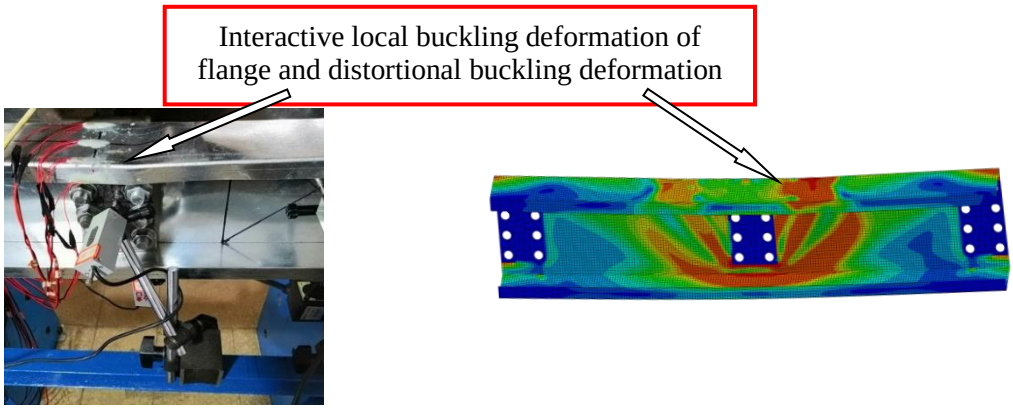

(a) Test result (b) FEA result

(1) Specimen H0-1.9-200-1010

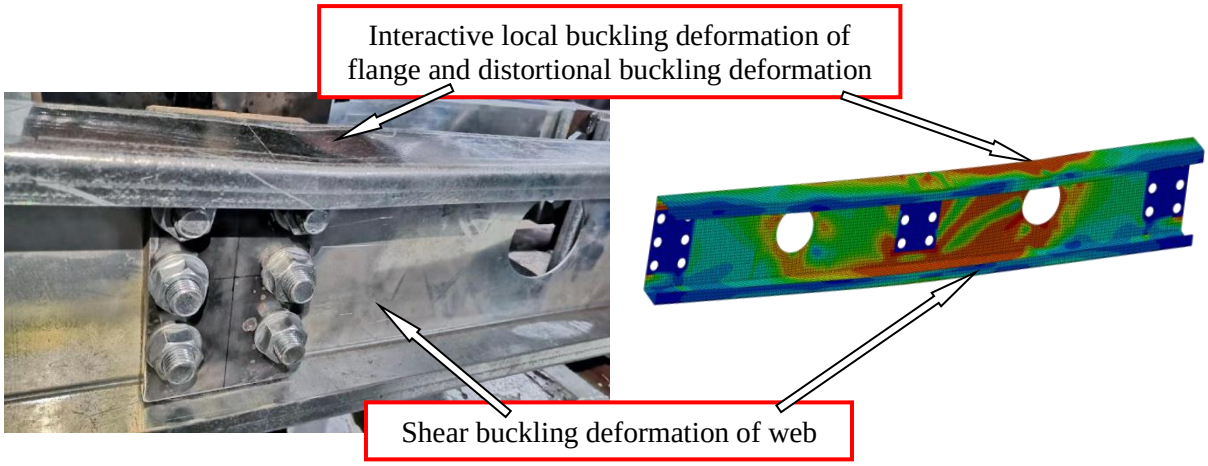

(a) Test result (b) FEA result

(2) Specimen H0.5-1.9-160-1170

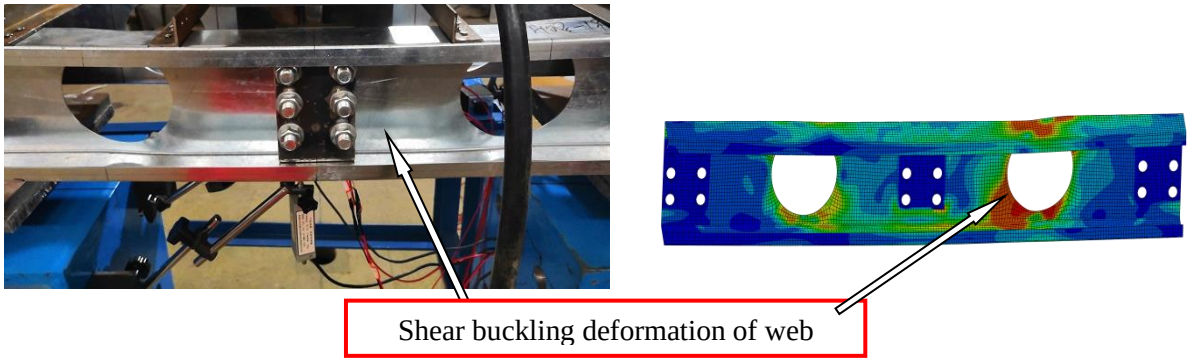

(a) Test result (b) FEA result

(3) Specimen H0.8-1.9-160-1010

Fig. 10 Comparison on failure mode of specimen from test and FEA

3.2.2. Ultimate bearing capacity

The results of the bearing capacity of specimen from FEA and test are presented in Table 2. It can be seen, the value of V_{EXP}/V_{FEA} is between 0.91 and 1.11, whose average value and coefficient of variation are 1.03 and 0.048, respectively, which shows that the FEA model adopted in this paper has high accuracy.

3.2.3. Load-deflection curves

The load-deflection curves of Hd_h/h-1.9-160-850 series and Hd_h/h-1.9-160-1010 series in test are compared with FEA results in Fig. 11. It can be seen, when the value of d_h/h is relatively smaller (0.35), the elastic stiffness of load-deflection curve in test is relatively smaller than that of FEA, and curve of specimen in test has a higher strength after buckling than that of FEA. When the value of d_h/h increases (0.50), the curves of FEA are in better agreement with those of test, which verifies rationality of FEA again.

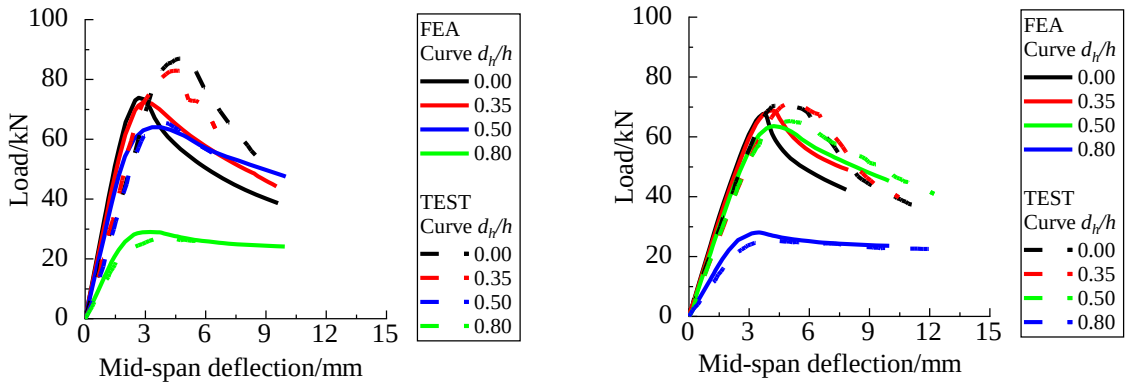

(a) Hd_h/h-1.9-160-850 (b) Hd_h/h-1.9-160-1010

Fig. 11 Load-deflection curves from test and FEA

4. Parametric study

4.1. Design of parameters

To conduct further research on the comprehensive performance of thin-walled web-perforated lipped C-shaped CFS beams under combined bending moment and shear force action, series of models verified above were adopted for further nonlinear parameter analysis. It is found from the test results that the two main factors that affect bearing capacity and failure mode of specimen are, respectively, the value of d_h/h and the value of a/h, and the value of h/t also affects the bearing capacity to a certain degree. Combined with tests design, h of the specimen for parameter analysis is designed as 100 mm, 120 mm, 140 mm, 160 mm, 180 mm, 200 mm and 300 mm, respectively, and the section thickness (t) of specimen was 1.9 mm, from which different value of h/t can be obtained. In addition, specimens with the h of 100 mm and 160 mm, additional specimens with t = 1.0 mm were designed. Due to that this paper mainly studies performance of web-perforated beams under combined bending moment and shear force action, the value of a/h of the specimens ranged from 1.5 to 4.0 with an increment of 0.5.

4.2. Influence of hole depth-to-web height ratio

The curve of the bearing capacity of specimen with the value of d_h/h is shown in Fig. 12. The curves are approximately horizontal at the beginning. When the value of d_h/h increases to a certain level, the curves drop sharply. At that time, bearing capacity shows more sensitivity to the change of the value of d_h/h.

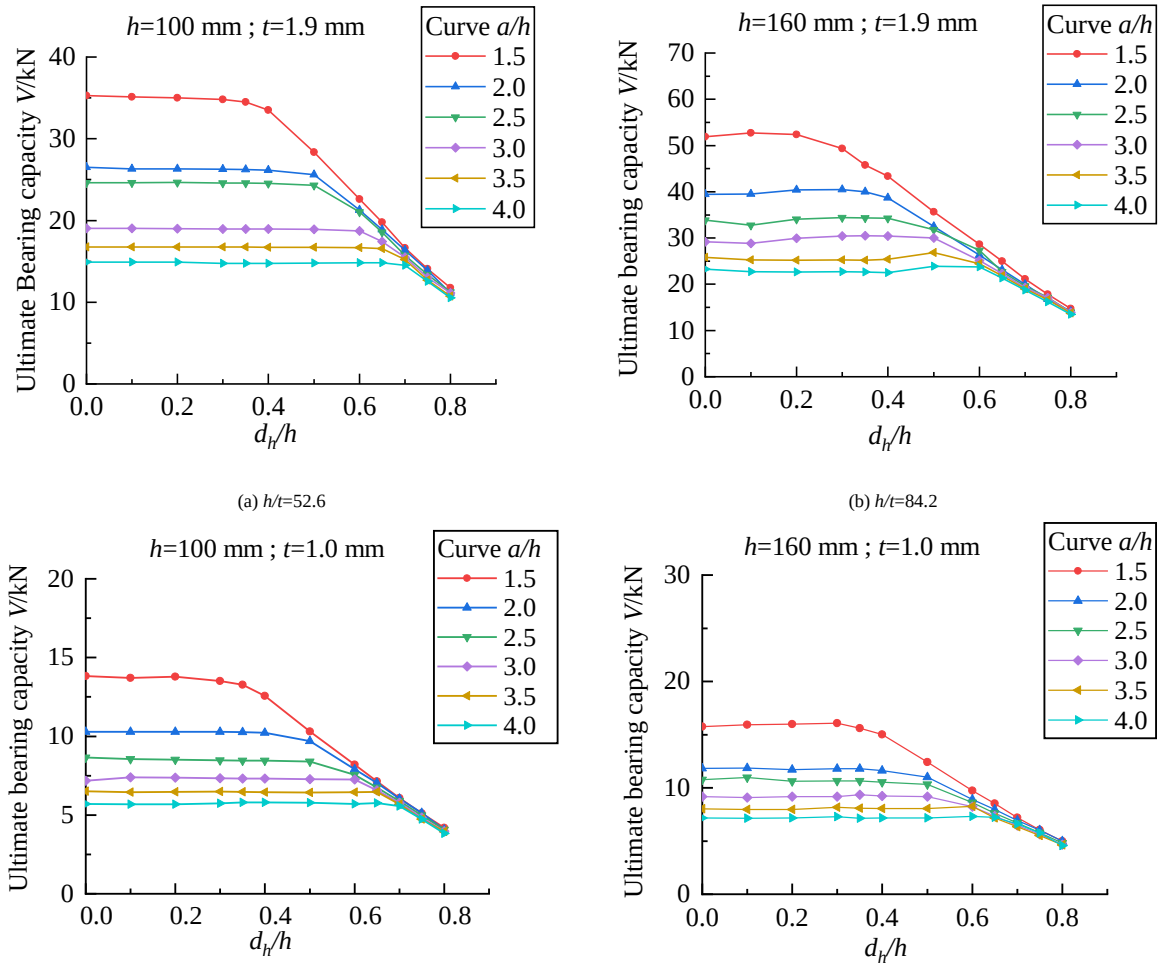

(a) h/t=52.6 (b) h/t=84.2

(c) h/t=100 (d) h/t=160

Fig. 12 Curves of bearing capacity with the value of d_h/h

Due to limited length, Hd_h/h-1.9-180-930 series (a/h = 2.0) are chosen for specific analysis. Fig. 13~15 shows the failure mode. For specimens with the value of $d_h/h \leq 0.35$, as seen from Fig. 13-(a) ~ (b), at mid-span section, there are obvious stress concentration areas in flange and along the shear failure direction in the shear-zone. As the value of d_h/h increases, the area of stress concentration in the shear zone increases. Specimens are subjected to the coupled bending and shear failure. As seen from Fig.14 -(a)~(b), interactive local buckling deformation and distortional buckling deformation occur at mid-span section. As seen from Fig.15-(a) ~ (b), slight local buckling deformation occurs in the shear zone along shear failure direction. For specimens with the value of d_h/h of 0.35 to 0.4, the area of stress concentration in the compression flange along the flange-width direction at mid-span decreases obviously, while the area along the span direction of specimen increases, and the failure mode begins to change. For specimens with the value of $d_h/h > 0.4$, as seen from Fig. 13-(c) ~ (d), the main area of stress concentration is in the web in shear zone along shear failure direction. As seen from Fig. 14-(c) ~ (d), interactive local buckling deformation and distortional buckling deformation occur at mid-span section. As seen from Fig. 15-(c) ~ (d), obvious local buckling deformation occurs near the web opening along shear failure direction. In conclusion, when the value of a/h= 2.0, as the value of d_h/h increases, failure mode of the steel beam changes from the coupled failure of bending and shear at mid-span into the shear failure of web local buckling in shear zone.

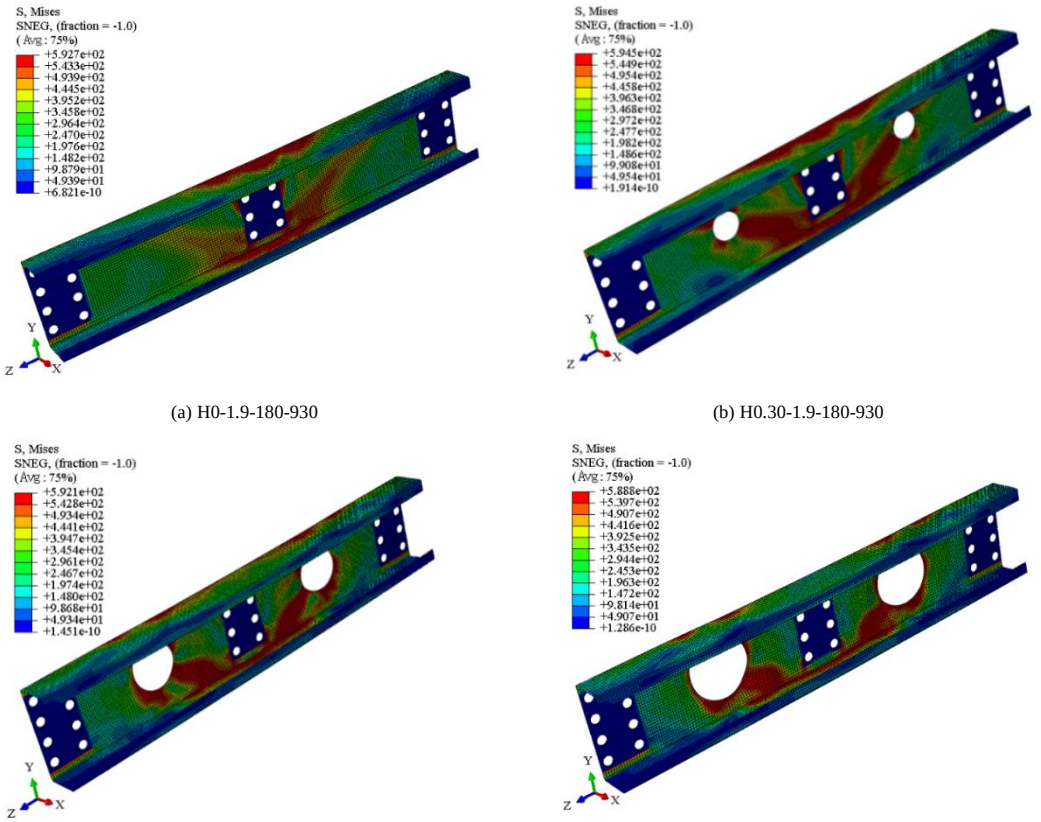

(a) H0-1.9-180-930 (b) H0.30-1.9-180-930

(c) H0.50-1.9-180-930 (d) H0.65-1.9-180-930

Fig. 13 Failure mode of series "Hd_h/h -1.9-180-930" with the value of d_h/h

(a) H0-1.9-180-930 (b) H0.3-1.9-180-930 (c) H0.5-1.9-180-930 (d) H0.65-1.9-180-930

Fig. 14 Buckling deformation of series "Hd_h/h-1.9-180-930" with the value of d_h/h

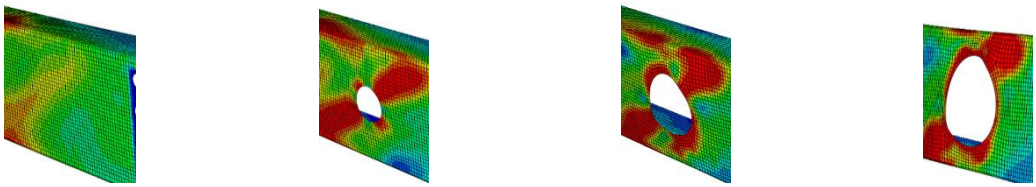

(a) H0-1.9-180-930 (b) H0.3-1.9-180-930 (c) H0.5-1.9-180-930 (d) H0.65-1.9-180-930

Fig. 15 Web buckling deformation of series "Hd_h/h-1.9-180-930" with the value of d_h/h

The mid-span load-deflection curve of Hd_h/h-1.9-180-930 series is shown in Fig. 16. When the value of $d_h/h \leq 0.35$, the curve has a fast drop after the peak point, indicating that failure of steel beam shows a certain suddenness. When the value of $d_h/h > 0.35$, the curve drops slower after the maximum point, which shows that the steel beam displays certain ductility after failure. The reason for that is when the value of d_h/h is relatively larger, more significant shear bucking deformation occur in the web, and the out-of-plane shear deformation weakens the overall unloading effect of the beams.

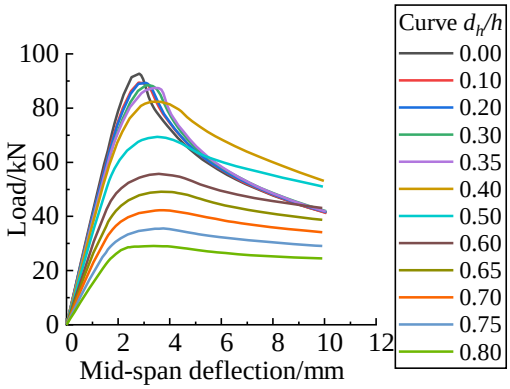

Fig. 16 Load-deflection curves of series "Hd_h/h-1.9-180-930" with the value of d_h/h (a/h=2.0)

4.3. Influence of web height-to-thickness ratio

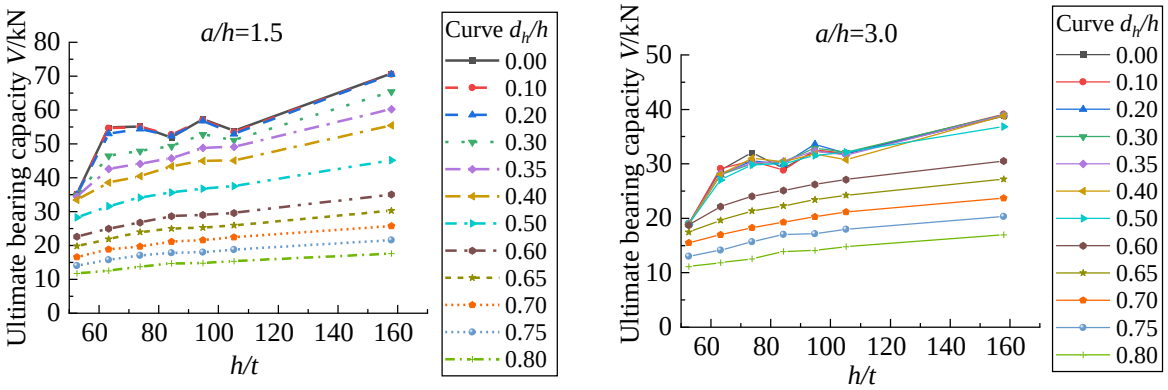

Fig. 17 Bearing capacity with the value of h/t (with different values of a/h, t=1.9 mm)

The curve of bearing capacity with the value of h/t is shown in Fig. 17. The specific analysis of bearing capacity corresponding to Fig. 17 is shown in Table 5. As seen from Fig. 18, with the value of d_h/h of 0 and 0.35, the bearing capacity shows more sensitivity to the change of the value of h/t. While with the value of d_h/h of 0.65 and 0.8, the bearing capacity is less affected by the value of h/t. The reasons can be explained that with a relatively smaller value of d_h/h, as the value of h/t increases, the ratio of plate width to plate thickness is easy to cross the critical value, thus failure mode transform from shear failure to local buckling failure. With a relatively larger value of d_h/h, area of shearing web core is deducted, and the shear stress for the remaining area above and below the web hole is smaller, which leads to that the influence of increase in the value of h/t on the bearing capacity is limited.

Table 5
Analysis of the effect of the value of h/t on bearing capacity of specimen

The value of a/h	Range of the value of d_h/h	Influence of the value of h/t on bearing capacity
1.5	$d_h/h \leqslant 0.2$	(1) High Coincidence degree of the curve ; (2) When the value of h/t is 52.6 ~ 73.7, 84.2 ~ 94.7 and 105.3 ~ 157.9, the bearing capacity increases as the increase of the value of h/t; (3) When the value of h/t is 73.7 ~ 84.2 and 94.7 ~ 105.3, bearing capacity decreases as the value of h/t increases.
3.0	$d_h/h \leqslant 0.5$	
1.5	$d_h/h > 0.2$	Bearing capacity increases with as the value of h/t increases, and the trend of the curve is similar.
3.0	$d_h/h > 0.5$	

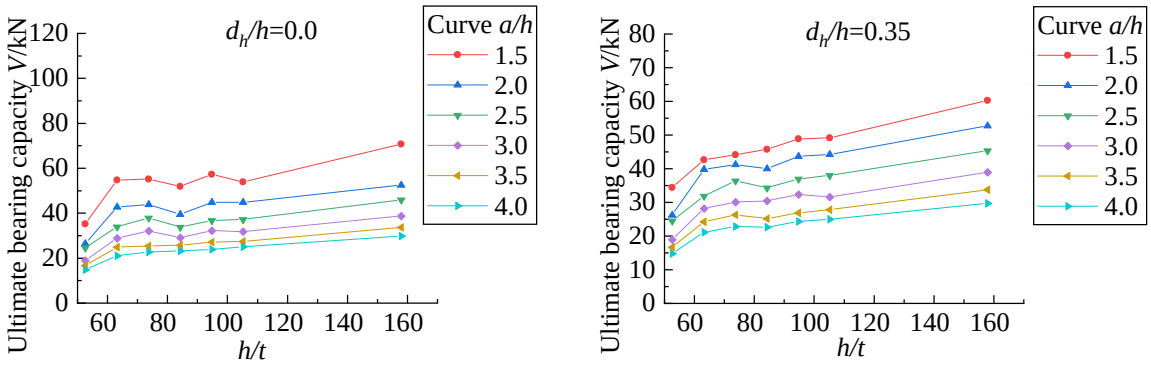

(a) (b)

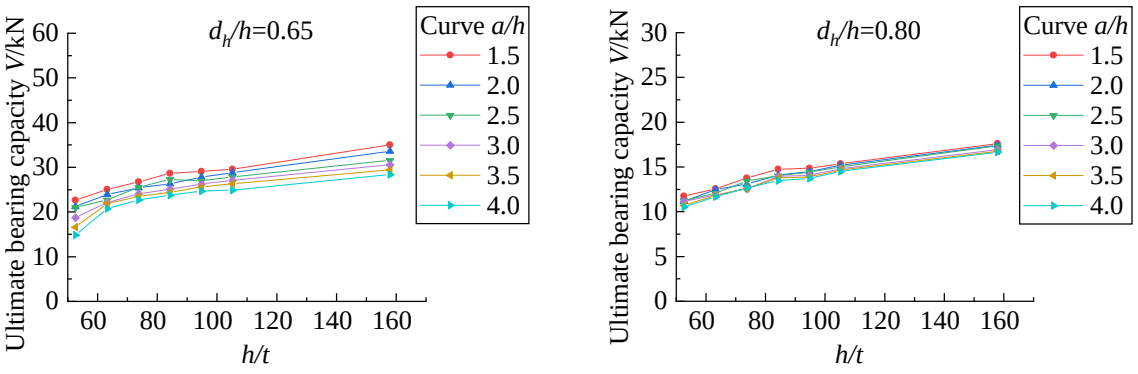

Fig. 18 Bearing capacity with the value of h/t (with different values of d_h/h, t=1.9 mm)

The variation of failure mode with the value of h/t of specimen with the value of a/h of 1.5 is shown in Fig. 19. As seen from Fig. 19-(a) ~ (b), with the value of d_h/h of 0.1 and relatively smaller value of h/t (h/t= 52.6 or 63.2), an obvious stress concentration area appears in flange and the web along shear failure direction at mid-span. As seen from Fig. 19 (a), maximum value of stress of specimen H0.10-1.9-100-510 at failure can reach the yield strength, which indicates material property of specimen is fully utilized. As seen from Fig. 19-(c) ~ (d), as the value of d_h/h increases, stress concentration area in the compression flange along flange-width direction at mid-span gradually decreases, while that along length direction of the steel beam gradually increases. And the maximum stress value at failure gradually decreases, which indicates that the steel beam is more prone to buckling. As seen from Fig. 20, when the value of d_h/h is 0.65, main area of stress concentration of specimen is in web shear failure direction, failure mode majors in shear failure, and the value of h/t barely affect the failure mode.

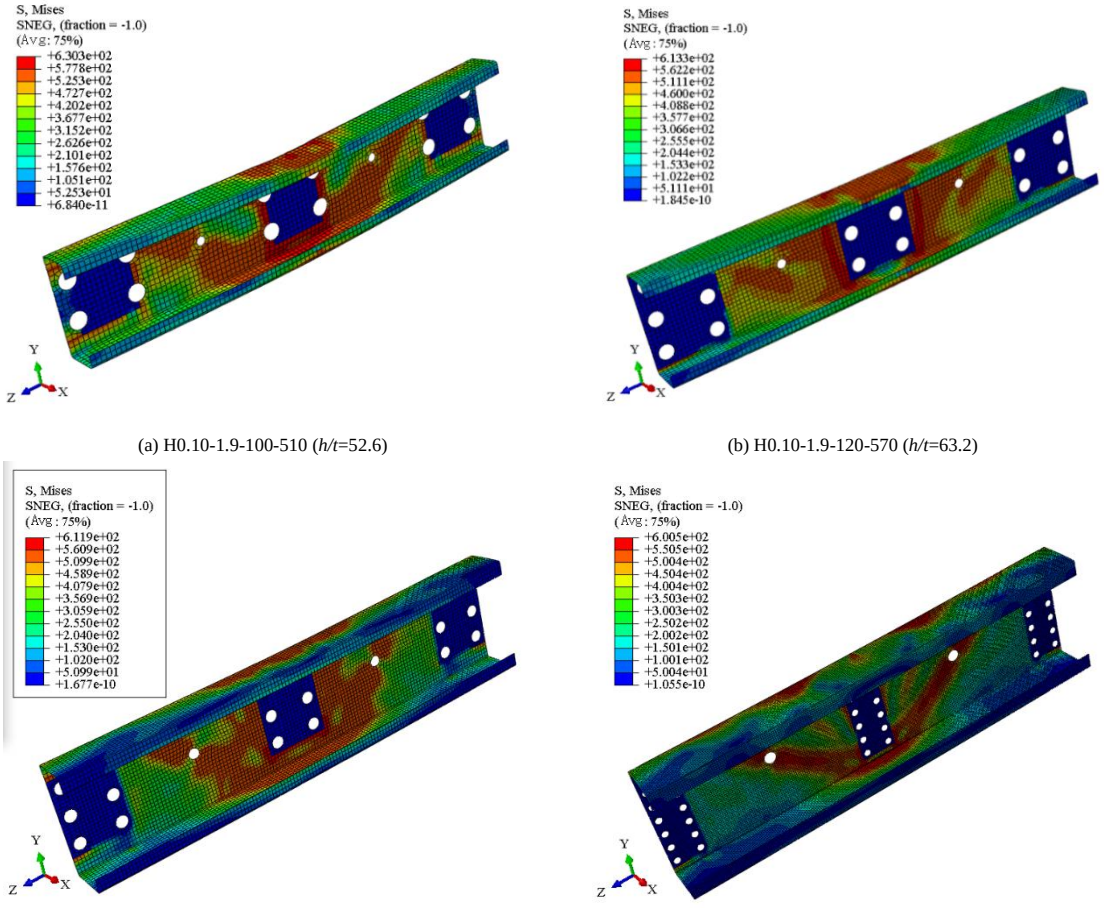

Fig. 19 Failure mode with the value of h/t (t = 1.9 mm; a/h = 1.5; d_h/h = 0.10)

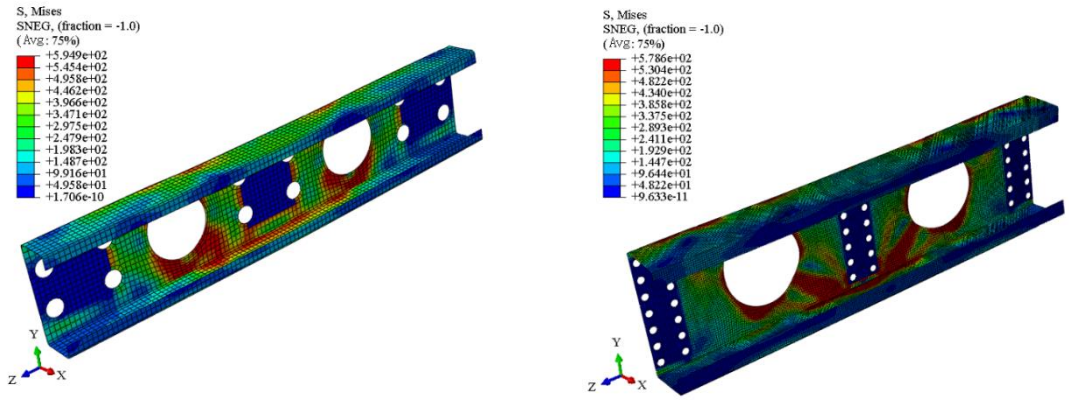

(a) H0.65-1.9-100-510(*h*/*t*=52.6) (b) H0.65-1.9-300-1110(*h*/*t*=157.3)

Fig. 20 Failure mode with the value of *h*/*t* (*t* = 1.9 mm; *a*/*h* = 1.5; d_h/h = 0.65)

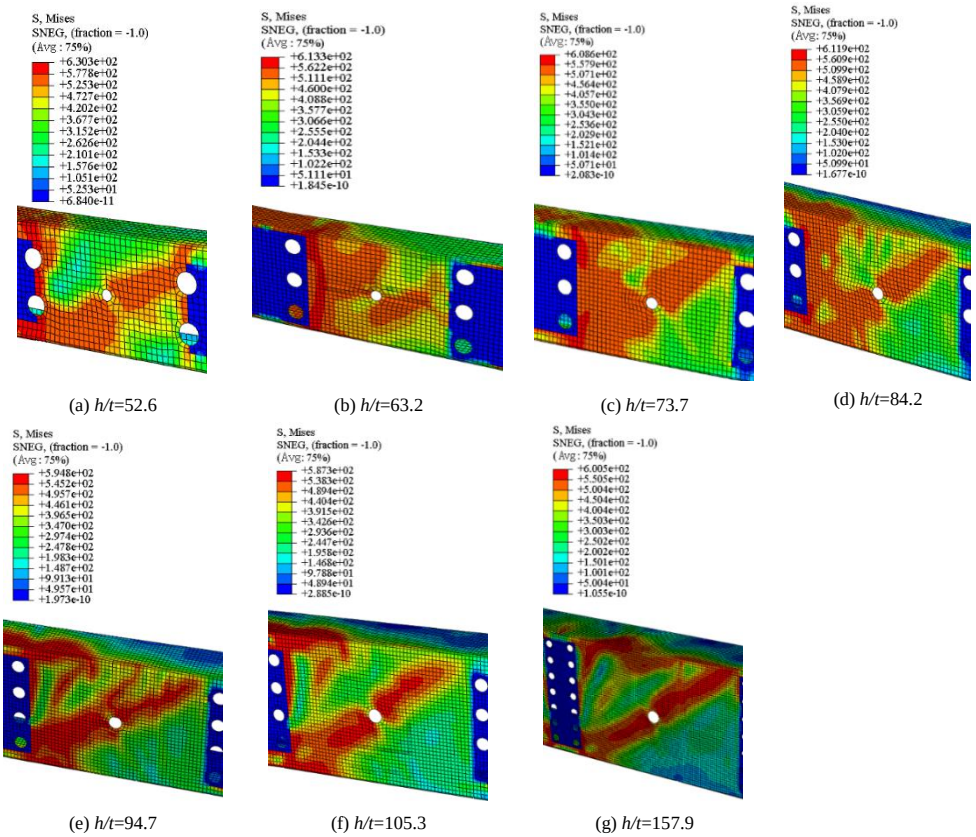

(a) *h*/*t*=52.6 (b) *h*/*t*=63.2 (c) *h*/*t*=73.7 (d) *h*/*t*=84.2

(e) *h*/*t*=94.7 (f) *h*/*t*=105.3 (g) *h*/*t*=157.9

Fig. 21 Web buckling deformation with the value of *h*/*t* (*t* = 1.9 mm; *a*/*h* = 1.5; d_h/h = 0.1)

Fig. 21 and Fig. 22 show that, buckling deformation in flange and the web in shear zone at mid-span with different values of *h*/*t*, respectively. As seen from Fig. 21, there is significant local buckling deformation in the web of steel beam with the value of *h*/*t* of 52.6, 84.2 and 105.3. As seen from Fig. 22, the web buckling deformation in shear zone of specimens with different values of *h*/*t* is similar. Combined with the above, when value of *h*/*t* increases from 73.7 to 84.2 and from 94.7 to 105.3, the curve of bearing capacity with value of *h*/*t* decreases due to flange local buckling deformation at mid-span, which shows that web local buckling has significant effect on the bearing capacity.

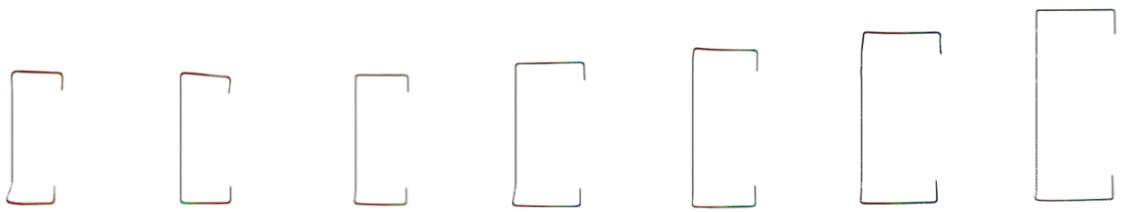

(a) *h*/*t*=52.6 (b) *h*/*t*=63.2 (c) *h*/*t*=73.7 (d) *h*/*t*=84.2 (e) *h*/*t*=94.7 (f) *h*/*t*=105.3 (g) *h*/*t*=157.9

Fig. 22 Flange buckling deformation with the value of *h*/*t* (*t*= 1.9 mm; *a*/*h* = 1.5; d_h/h = 0.1)

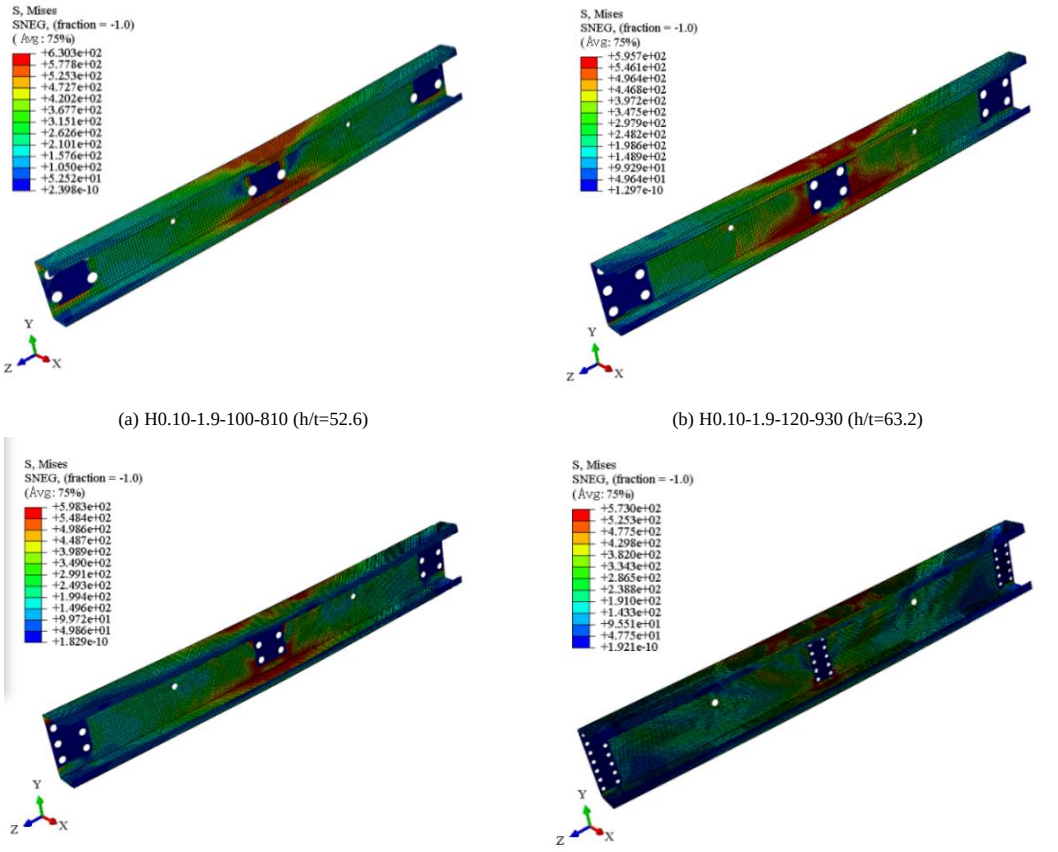

(a) H0.10-1.9-100-810 (h/t=52.6)

(b) H0.10-1.9-120-930 (h/t=63.2)

(c) H0.10-1.9-160-1170 (h/t=84.2)

(d) H0.10-1.9-300-2010 (h/t=157.3)

Fig. 23 Failure mode with the value of h/t (a/h = 3.0; d_h/h = 0.10)

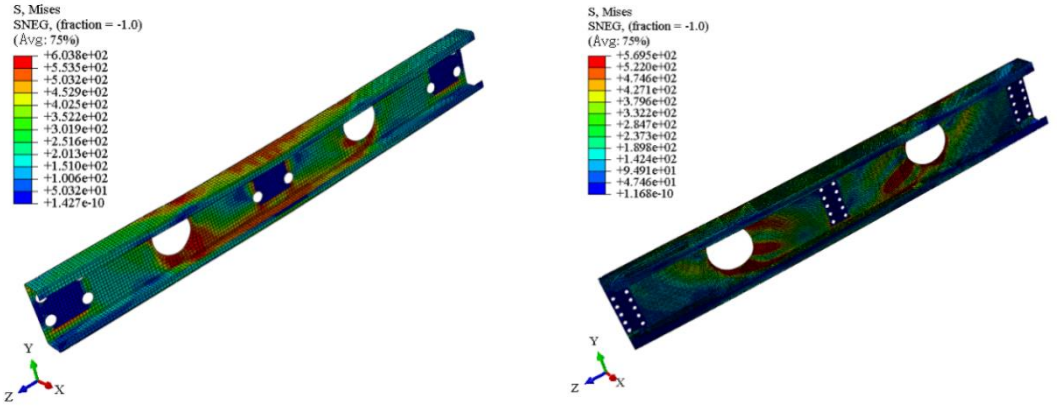

(a) H0.65-1.9-100-810 (h/t=52.6)

(b) H0.65-1.9-300-2010 (h/t=157.3)

Fig. 24 Failure mode with the value of h/t (a/h = 3.0; d_h/h = 0.65)

Fig. 23 shows the failure mode with the value of h/t of specimen with the value of a/h of 3.0. As seen from the figure, with the value of d_h/h of 0.1, the failure mode of specimen with different the values of h/t are mainly bending failure at mid-span, the shear failure in web is not significant, and there is an obvious flange stress concentration at mid-span which decreases as the value of h/t increases. As seen from Fig. 24, with the value of d_h/h of 0.65, as the increase of the value of h/t, stress concentration area tend to be located in the web shear failure direction, and failure mode transforms from the coupled failure of bending and shear to the shear failure.

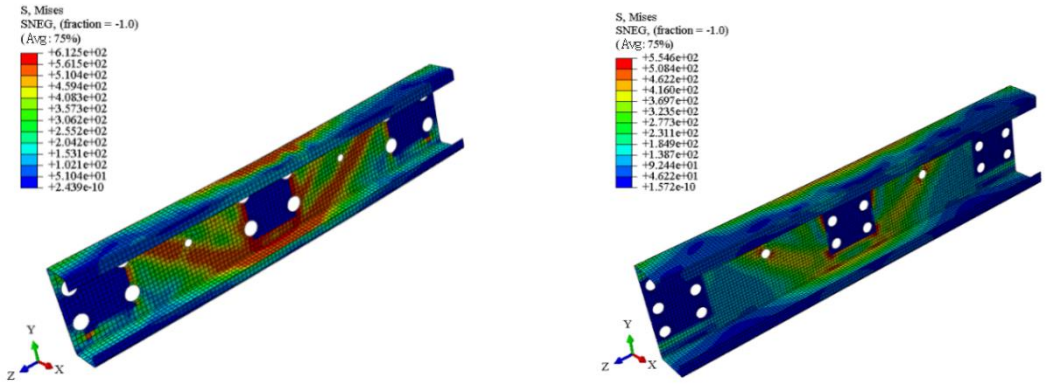

(a) H0.10-1.0-100-510 (h/t=100) (b) H0.10-1.0-160-690 (h/t=160)

Fig. 25 Failure mode with t =1.0 mm (a/h = 1.5)

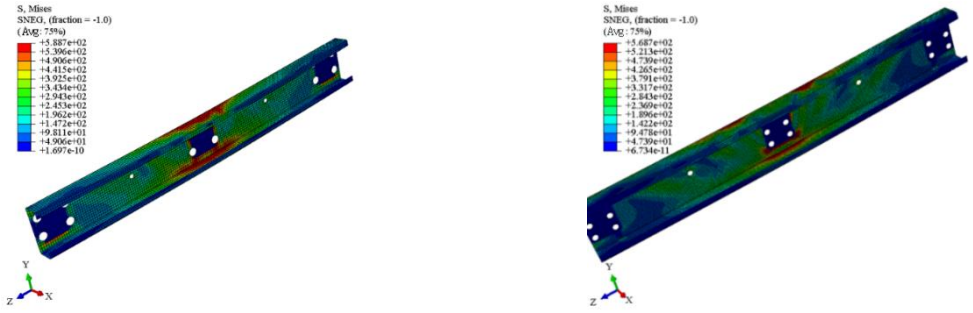

(a) H0.10-1.0-100-810 (h/t=100) (b) H0.10-1.0-160-1170 (h/t=160)

Fig. 26 Failure mode with t =1.0 mm (a/h = 3.0)

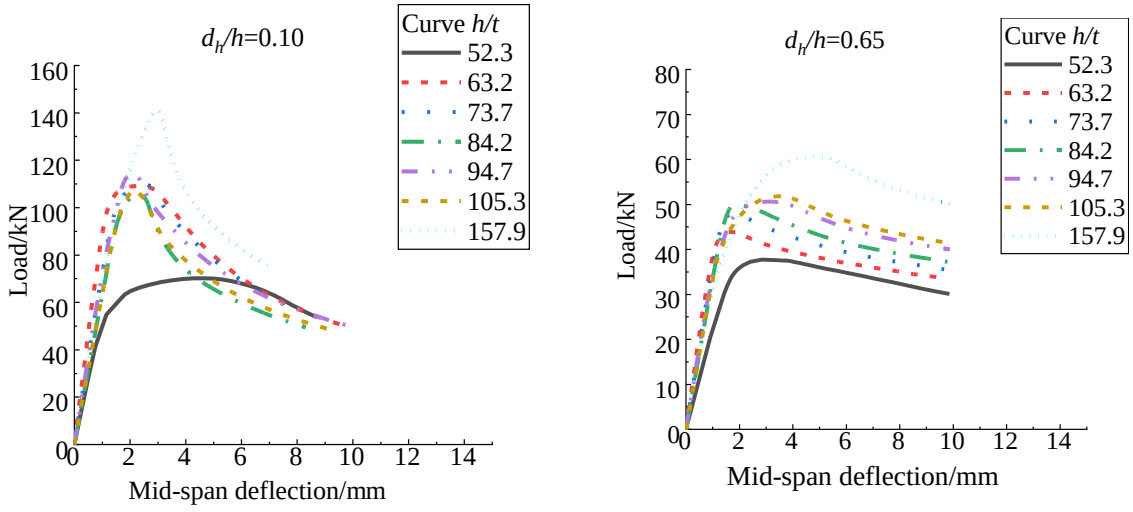

(a) d_h/h=0.10 (b) d_h/h=0.65

Fig. 27 Load-deflection curves with the value of h/t (t= 1.9 mm, a/h=1.5)

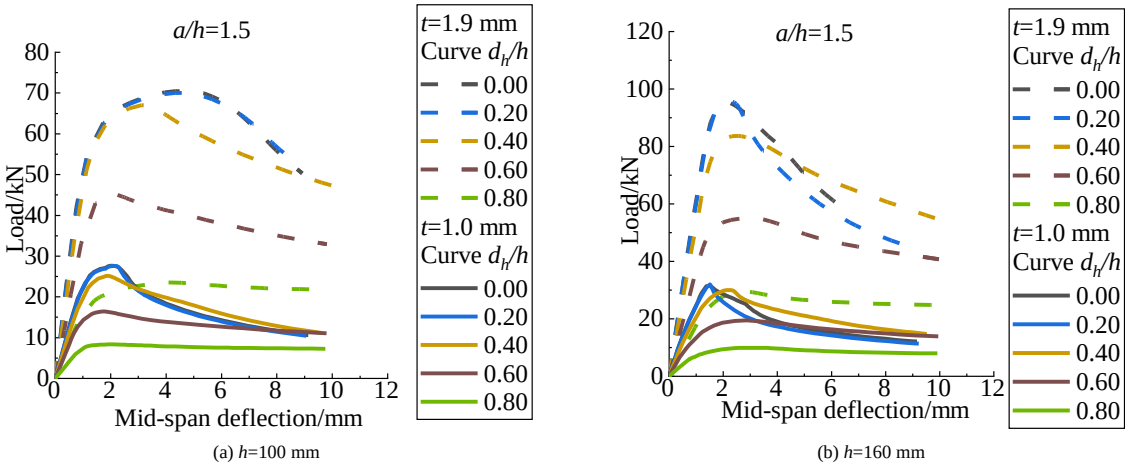

(a) h=100 mm (b) h=160 mm

Fig. 28 Load-deflection curves with the value of h/t (with same h)

The failure mode of specimen with t = 1.0 mm under the same conditions with those of specimens in Fig. 19 and Fig. 23 are respectively presented in Fig. 25 and Fig. 26. As seen from the figure, as t changes from 1.9 mm to 1.0 mm, the stress concentration area of the specimen decreases.

The load-deflection curve with the value of h/t is presented in Fig. 27 and Fig. 28. As seen from Fig. 27 that with same t= 1.9 mm, specimen with the value of h/t of 52.6 has the lowest stiffness, the beam with the value of h/t of 63.2 has the highest stiffness, and the stiffness increases the most as the value of h/t increases from 52.6 to 63.2. As seen from Fig. 28, when t changes from 1.9 mm to 1.0 mm, as the value of h/t increases, the stiffness decreases significantly, and the post-buckling strength of specimen with h = 100 mm also decreases.

4.4. Influence of shear-span ratio

Fig. 29 shows curve of the bearing capacity of specimen with the value of a/h, and analysis is presented in Table 6. According to Section 3.2 that when the value of d_h/h is relatively larger, the bearing capacity is determined by the value of d_h/h. In hence, for steel beam dominated by shear failure due to the opening of super large holes (d_h/h > 0.5), the value of a/h barely affect the bearing capacity.

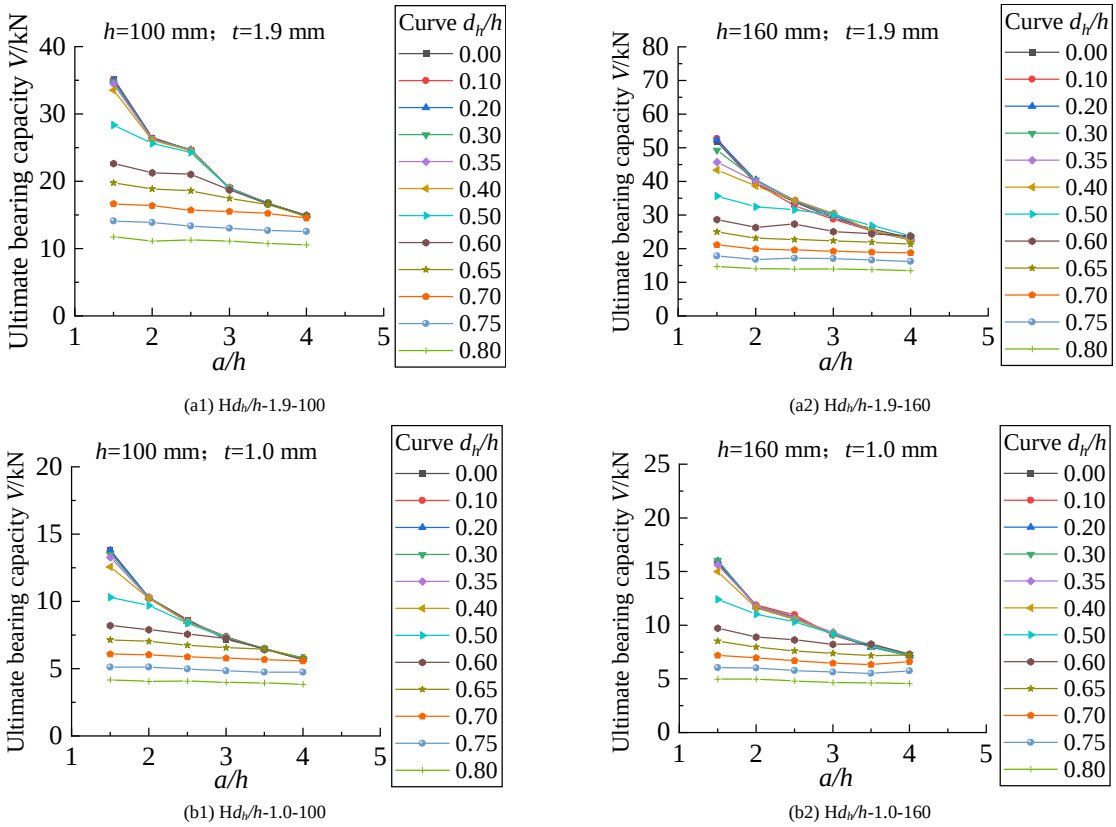

(a1) Hd_h/h-1.9-100 (a2) Hd_h/h-1.9-160

(b1) Hd_h/h-1.0-100 (b2) Hd_h/h-1.0-160

Fig. 29 Bearing capacity with the value of a/h

Table 6
Analysis of the influence of the value of d_h/h on the bearing capacity of specimen

Range of the value of h/t	Range of the value of d_h/h	Influence of the value of a/h on bearing capacity of specimen
h/t = 52.6	$d_h/h \leqslant 0.40$	The curves is highly overlapped, and bearing capacity shows sensitivity to the change of the value of a/h.
h/t > 52.6	$d_h/h \leqslant 0.20$	
h/t = 52.6	$0.4 < d_h/h \leqslant 0.65$	The curves begin to deviate, and the influence of variation of the value of a/h on bearing capacity decreases as the value of d_h/h increases.
h/t > 52.6	$0.2 < d_h/h \leqslant 0.50$	
h/t = 52.6	d_h/h > 0.65	The change of the value of a/h has the least influence on bearing capacity, the curve is close to the horizontal state.
h/t > 52.6	d_h/h > 0.50	

Take specimens with the value of h/t of 52.6 (h= 100 mm, t= 1.9 mm) and the value of d_h/h of 0.2 and 0.75 as examples, the specific analysis on the variation of failure modes of steel beams with the value of a/h is as following.

When the value of h/t of specimen is 52.6 (h= 100 mm, t= 1.9 mm), as seen from Fig. 30, with the value of d_h/h of 0.2, the variation of flange stress distribution at mid-span is less affected by the value of a/h, and the area of web stress concentration in the shear zone shrinks as the value of a/h increases, which shows that failure mode of specimen gradually changes from the coupled failure of bending and shear to the mainly bending failure as the value of a/h increases. As seen in Fig. 31, for specimens with the value of d_h/h of 0.75, the failure mode is less affected by the value of a/h, and the stress is mainly concentrated near the web opening. With the increase of the value of a/h, slight stress concentration appears in the compression flange above the hole

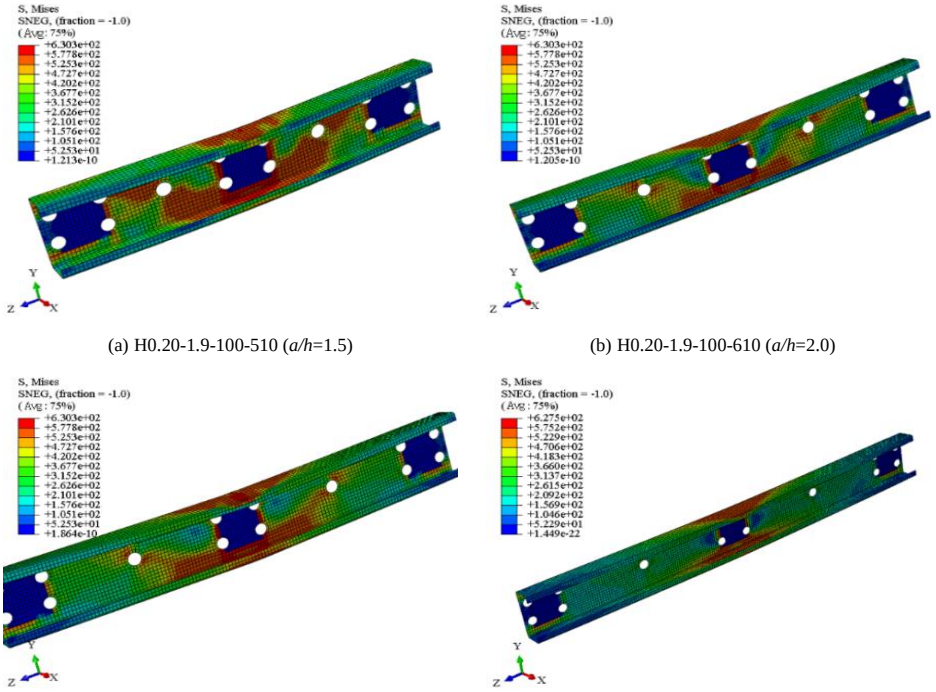

(a) H0.20-1.9-100-510 (a/h=1.5) (b) H0.20-1.9-100-610 (a/h=2.0)

(c) H0.20-1.9-100-710 (a/h=2.5) (d) H0.20-1.9-100-910 (a/h=3.5)

Fig. 30 Failure mode with the value of a/h (h= 100 mm; t= 1.9 mm; d_h/h= 0.20)

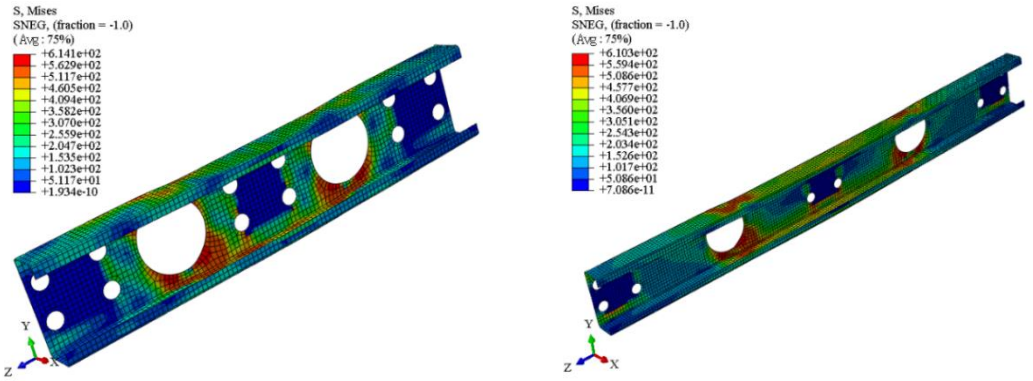

(a) H0.75-1.9-100-510 (a/h=1.5) (b) H0.75-1.9-100-910 (a/h=3.5)

Fig. 31 Failure mode with the value of a/h (h= 100 mm; t= 1.9 mm; d_h/h= 0.75)

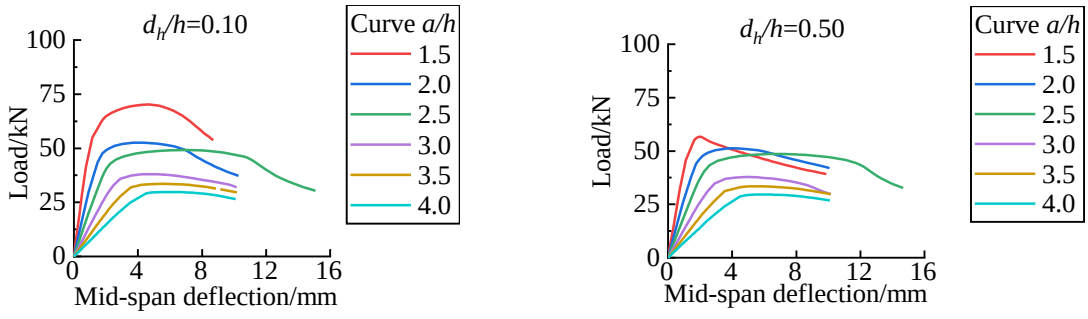

(a) (b)

Fig. 32 Load-deflection curves with the value of a/h (h/t =52.6)

Fig. 32 shows the load-deflection curve with the value of a/h, under the condition that the value of h/t is 52.6 (h= 100 mm, t= 1.9 mm) and the values of d_h/h are 0.1 and 0.5, respectively. As can be seen, stiffness of specimen drops as the increase of the value of a/h, which is due to that effect of bending moment also getting larger as the increase of the value of a/h.

4.5. Classification of failure mode of web perforated beam in combined bending and shear action

According to the analysis above, the bending-shear members studied in this paper have three types of failure modes, which are respectively the mainly shear failure, the mainly bending failure and the coupled failure of bending and shear.

The specimen subjected to mainly shear failure has the following characteristics: (1) The failure mode is dominated by local web shear buckling in the shear zone. (2) The bearing capacity shows sensitivity to the change of the value of d_h/h, and the corresponding bearing capacity is located at where the curve of bearing capacity against the value of d_h/h starts decreasing linearly.

The bearing capacity of web perforated specimen is close to that of solid-web specimen when it is subjected to mainly bending failure, thus the bearing capacity of steel beam can be mainly predicted according to the failure mode.

For beams subjected to the bending failure, flange stress concentration appears at mid-span, while web stress concentration is not significant. For beams subjected to the coupled failure of bending and shear, obvious stress concentration appears in both flange and web.

According to the characteristics of these three basic failure modes, Table 7 summarizes the classification of the failure modes of web perforated thin-walled C-shaped CFS bending-shear members with different loading conditions and geometric parameters.

Table 7
Classification of the failure mode of web perforated thin-walled C-shaped CFS beams under combined bending moment and shear force action

Failure mode	Demarcation conditions (Parameters range)
Mainly shear failure	(1) The value of a/h: $1.5 \leqslant a/h \leqslant 2.0$, and the value of d_h/h: $d_h/h \geqslant 0.60$; (2) The value of a/h: $2.0 < a/h \leqslant 4.0$, and the value of d_h/h: $d_h/h \geqslant 0.65$.
Coupled failure of bending and shear	Beams beyond the scope of parameters of steel beams with mainly shear failure and mainly bending failure in this Table.
Mainly bending failure	The value of a/h: $2.5 < a/h \leqslant 4$, and the value of d_h/h: $d_h/h \leqslant 0.2$.

5. Conclusions

This paper presents tests on 20 groups of thin-walled web perforated C-shaped CFS beams under combined bending moment and shear force action and the FEA by means of ABAQUS. The rationality of the model was verified by comparing results from test and FEA. Then refined parameter analysis was conducted on the three factors as follows: the value of d_h/h, the value of h/t and the value of a/h. On basis of that, failure modes of web perforated thin-walled C-shaped CFS beams under combined bending moment and shear force action were classified, and several conclusions were put ward as following:

(1) The value of d_h/h has a decisive effect on bearing capacity and failure mode of specimen. With the increase of the value of d_h/h, the failure mode of the steel beam transforms from the coupled failure of bending and shear to the shear failure, or from the bending failure to the coupled failure of bending and shear and then to the shear failure.

(2) The value of h/t affects failure mode of specimen mainly subjected to the bending failure and the coupled failure of bending and shear to a certain degree. With the increase of value of h/t, the stress concentration area decreases. With the same h, bearing capacity and stiffness of the specimen decrease as the value of h/t increases.

(3) The value of a/h affects failure mode of specimen mainly subjected to the bending failure and the coupled failure of bending and shear to a certain degree. With the increase of the value of a/h, web stress concentration in in shear zone and stiffness of specimen decrease. With a relatively smaller value of d_h/h ($d_h/h \leq 0.5$), bearing capacity shows more sensitivity to the change of the value of a/h, and bearing capacity drops as the increase of the value of a/h.

Acknowledgement

The authors are appreciated for the funding and support from the National Natural Science Foundation of China (Grant No. 51608538), Testing Research Funding from Hunan Tieyuan Civil Engineering Testing Co., Ltd (HNTY2021K02) and Natural Science Foundation of Hunan Province (2021JJ50029).

References

[1] Langan J E., Laboube R A., YU W., Structural behavior of perforated web elements of cold-formed steel flexural members subjected to web crippling and a combination of web crippling and bending[D]. University of Missouri-Rolla, 1994.
[2] Uphoff C, Laboube R A, YU W., Structural behavior of circular holes in web elements of cold-formed steel flexural members subjected to web crippling for End-One-Flange loading[D]. University of Missouri-Rolla, 1996.
[3] Eiler M, Laboube R, YU W., Behavior of web elements with openings subjected to linearly varying shear[D]. University of Missouri-Rolla, 1997.
[4] North American specification for the design of cold-formed steel structural members: AISI-S100-2016[S]. Washington: American Iron and Steel Institute, 2016.
[5] Standards Australia/Standards New Zealand (SA). Australia/New Zealand standard A S/NZS4600 cold-formed steel structures, Sydney, Australia; 2005.
[6] Schafer B W, Pekoz T., Laterally braced cold-formed steel flexural members with edge stiffened flanges[J]. Journal of Structural Engineering-ASCE, 1999, 125(2): 118-127.
[7] Schafer B W., Local, distortional, and Euler buckling of thin-walled columns[J]. Journal Of Structural Engineering-ASCE, 2002, 128(3): 289-299.
[8] YU C, Schafer B W., Distortional buckling tests on cold-formed steel beams[J]. Journal Of Structural Engineering, 2006, 132(4): 515-528.
[9] Schafer B.W., Direct strength method design guide[Z]. Washington. American Iron and Steel Institute, 2006.
[10] Moen C D., Direct strength design of cold-formed steel members with perforations[D]. The Johns Hopkins University, 2009.
[11] Moen C D, Schafer B W., Elastic buckling of cold-formed steel columns and beams with holes[J]. Engineering Structures, 2009, 31(12): 2812-2824.
[12] Moen C D, Schafer B W., Elastic buckling of thin plates with holes in compression or bending[J]. Thin-Walled Structures, 2009, 47(12): 1597-1607.
[13] Moen C D, Schudlich A, von der Heyden A., Experiments on cold-formed steel C-shaped joists with unstiffened web holes[J]. Journal of Structural Engineering, 2013, 139(5): 695-704.
[14] Pham C H, Hancock G J., Direct strength design of cold-formed C-shapeds for shear and combined actions[J]. Journal of Structural Engineering, 2012, 138(6): 759-768.
[15] Keerthan P, Hughes D, Mahendran M., Experimental studies of hollow flange channel beams subject to combined bending and shear actions[J]. Thin-Walled Structures, 2014, 77: 129-140.
[16] Keerthan P, Mahendran M, Hughes D., Numerical studies and design of hollow flange channel beams subject to combined bending and shear actions[J]. Engineering structures, 2014, 75: 197-212.
[17] Faridmehr I, Tahir M M, Osman M H, et al., An experimental investigation of stiffened cold-formed C-channels in pure bending and primarily shear conditions[J]. Thin-Walled Structures, 2015, 96: 39-48.
[18] Wang L, Young B., Beam tests of cold-formed steel built-up sections with web perforations[J]. Journal of Constructional Steel Research, 2015, 115: 18-33.
[19] Wang L, Young B. Design of cold-formed steel built-up sections with web perforations subjected to bending[J]. Thin-Walled Structures, 2017, 120: 458-469.
[20] Pham S H, Pham C H, Hancock G J., Experimental study of shear strength of cold-formed channels with an aspect ratio of 2.0[J]. Journal of Constructional Steel Research, 2018, 149: 141-152.
[21] Pham S H, Pham C H, Rogers C A, et al., Experimental validation of the Direct Strength Method for shear spans with high aspect ratios[J]. Journal of Constructional Steel Research, 2019, 157: 143-150.
[22] Degtyareva N, Gatheeshgar P, Poologanathan K, et al., Combined bending and shear behaviour of slotted perforated steel channels: Numerical studies[J]. Journal of Constructional Steel Research, 2019, 161: 369-384.
[23] Lawson R M, Basta A., Deflection of C section beams with circular web openings[J]. Thin-Walled Structures, 2019, 134: 277-290.
[24] Pham D K, Pham C H, Pham S H, et al., Experimental investigation of high strength cold-formed channel sections in shear with rectangular and slotted web openings[J]. Journal of Constructional Steel Research, 2020, 165: 10588.
[25] Wang L, Li J, Luo C, et al. Experimental and numerical study on the shear behavior of web perforated cold-formed steel beams[J]. Structures, 2022, 45: 2117-2136.